ACS Partner Journal

Journal of the American Society for Mass Spectrometry

pubs.acs.org/jasms

Research Article

Top-Down Analysis of Supercharged Proteins Using Collision-, Electron-, and Photon-Based Activation Methods

Published as part of the Journal of the American Society for Mass Spectrometry virtual special issue "Focus: Ion Chemistry and Electrospray Ionization".

Kyle J. Juetten and Jennifer S. Brodbelt*

Cite This: J. Am. Soc. Mass Spectrom. 2023, 34, 1467−1476

Read Online

ACCESS | Metrics & More | Article Recommendations | Supporting Information

ABSTRACT: The impact of supercharging on the fragmentation patterns of six proteins, ubiquitin, cytochrome c, staph nuclease, myoglobin, dihydrofolate reductase, and carbonic anhydrase, was investigated for five activation methods, HCD, ETD, EThcD, 213 nm UVPD, and 193 nm UVPD under denaturing conditions. Changes in sequence coverage, alterations in the number and abundance of preferential cleavages (N-terminal to proline, C-terminal to aspartic or glutamic acid, adjacent to aromatic residues), and changes in individual fragment ion abundances were evaluated. Large decreases in sequence coverage were observed upon supercharging of proteins activated by HCD, whereas modest gains were observed for ETD. Minimal changes in sequence coverage were observed when using EThcD, 213 nm UVPD, and 193 nm UVPD, all of which tended to display the highest sequence coverages of the activation methods. Specific preferential backbone cleavage sites were increasingly enhanced for all proteins in supercharged states for all activation methods, particularly for HCD, 213 nm UVPD, and 193 nm UVPD. Even if large gains in sequence coverages were not apparent for the highest charge states, supercharging consistently led to at least a few new backbone cleavage sites for ETD, EThcD, 213 nm UVPD, and 193 nm UVPD for all proteins.

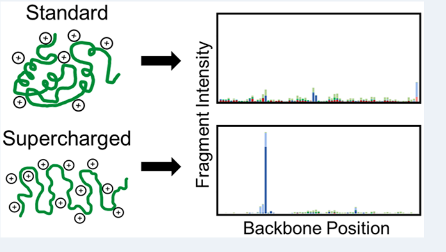

■ INTRODUCTION

Advances in top-down mass spectrometry have expanded its adoption for proteome research.[1−3] This approach offers the potential for identification of sequence truncations, single nucleotide polymorphisms, and combinatorial post-translational modifications (PTMs),[1−3] all features which can affect the activities, functions, and structures of proteins and which can be challenging to pinpoint using conventional bottom-up approaches.[4,5] Characterization of such features by top-down approaches requires activation methods that promote numerous backbone cleavages of the protein to afford high sequence coverage and yet do not dislodge labile modifications.[6] In addition to the popular conventional collisional activation methods, other methods that have shown significant success for analysis of intact proteins include electron-activated dissociation[7] and ultraviolet photodissociation (UVPD).[8] The extent and scope of fragmentation is governed by numerous factors such as the activation method used and both protein charge state and its primary sequence.[9−12] Understanding how these factors affect protein fragmentation has been explored in several foundational studies[9,12−15] and is critical for designing predictive rules, aiding interpretation of MS/MS spectra, and implementing the optimal experimental parameters for maximizing the information obtained from top-down proteomics strategies.

Seminal investigations of the fragmentation of peptides based on collisional activation resulted in the development of the mobile proton model, which provides a foundation for understanding fragmentation according to charge location and density.[16,17] It was recognized that the number and locations of protons of a protonated peptide modulate its fragmentation, particularly influenced by the presence of basic amino acids which can sequester protons and mediate the initiation of charge-directed fragmentation.[18] As the interest and feasibility of analyzing intact proteins has grown, more attention has been directed toward uncovering the factors that impact protein fragmentation.[12−15,19−25] Key studies examining the relationship between precursor charge state and the dissociation of intact proteins found that the relative number of charges on a protein influenced whether fragmentation was directed primarily toward neutral losses and backbone cleavages C-terminal to acidic residues (for lower charge states or proteins with few mobile protons) or toward backbone cleavages N-terminal to proline in addition to more nonspecific amide

Received: April 13, 2023
Revised: May 26, 2023
Accepted: June 9, 2023
Published: June 26, 2023

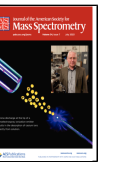

backbone cleavages (for high charge states with more mobile protons).[13,20−22] This line of inquiry was extended by employing guanidination of lysines, reinforcing the idea that cleavage of the protein backbone was enhanced C-terminal to acidic residues for proteins with restricted proton mobility.[23] The enhancement of preferential backbone cleavages has been exploited in a top-down strategy that used proton transfer charge reduction reactions to consolidate proteins into one lower charge state prior to CID, thus enhancing cleavages occurring C-terminal to acidic residues, yielding simpler MS/MS spectra and boosting dynamic range for protein identification.[26] The analysis of fragmentation propensities was further expanded to include the impact of a protein's higher order structure, revealing that backbone cleavages adjacent to acidic or aromatic residues were enhanced for proteins in native-like folded conformations.[24,25] These trends varied according to the activation method used.[7,12,27−35] Methods like electron capture or electron transfer dissociation displayed nonspecific backbone cleavages regardless of charge state; however, the extent and efficiency of fragmentation was heavily influenced by precursor charge state.[7,27] Previous top-down studies showcased this effect as the sequence coverage and the number of matched fragments increased for proteins when activated using ETD as charge state increased.[28,29] When utilizing ETD for characterization of ions in low charge states, nondissociative electron transfer is often predominant, resulting in inefficient conversion of precursor ions to product ions and necessitating the need for additional supplemental activation.[30,31] Previous studies have shown that EThcD and AI-ETD largely outperform ETD in both the number of generated fragments and overall sequence coverage when compared to ETD of low charge states for a variety of proteins.[32] Another study which used carbamylation as a means of manipulating precursor charge state showed that a reduction in protein charge state had a negative impact on the sequence coverage obtained from collision-based MS/MS approaches, primarily by reducing the number of backbone cleavage sites, while UVPD exhibited minimal deleterious effects as a function of charge state.[33] This trend was also explored in a study that examined several ways to reduce the charge states of proteins (e.g., proton transfer charge reduction, analysis of low charge states produced by native or basic solution conditions, or by carbamylation of basic lysine sites), and in all cases sequence coverages diminished for lower charge states upon collisional activation but not by 193 nm UVPD.[12] One recent investigation which focused on using 213 nm UVPD to aid in proteome identifications found that key diagnostic ions, such as $y-2$ ions, are prevalent regardless of precursor charge state and occur predominantly via cleavages at the N-terminal to proline.[34] Correlations between the fragment types and sequence coverages were also examined in a study that compared the outcome of using 193 nm versus 213 nm photons for UVPD, revealing that $y-2$ and a ions originating from fragmentation next to proline residues were more notably enhanced for 213 nm UVPD relative to 193 nm UVPD.[35]

Owing to the recognized importance of charge state on the fragmentation of proteins, numerous methods to manipulate charging of proteins have been explored. Charge reduction of proteins can be implemented by changing the solution conditions used for ESI[36−38] or by proton transfer charge reduction in the gas phase.[39] Increasing the charge states of proteins is another tactic typically enabled by addition of solution modifiers prior to ESI[40−44] resulting in the production of "supercharged" ions. Examples of commonly used supercharging agents include *m*-nitrobenzyl alcohol, sulfolane, and ethylene carbonate, among others.[45−49] The mechanism of supercharging is still under investigation. The use of these agents can improve mass spectrometry analyses of proteins by shifting the m/z of the ions to a less congested region, separating overlapping ions, in some cases consolidating ion current into fewer charge states or increasing fragmentation efficiency during MS/MS. Supercharging may also lead to significant changes in protein fragmentation, offering the potential to increase the information harvested from top-down MS/MS analysis. For example, one study showed that supercharging can result in the funneling of fragmentation into a few dominant backbone cleavages while reducing the abundance of fragmentation at neighboring residues.[50] Supercharging of proteins also resulted in more efficient cleavage of disulfide bonds and overall greater fragmentation efficiency for ECD and CAD.[51]

Herein, we investigate the effects of supercharging agents on the fragmentation of six proteins ranging in molecular size from 8.6 to 29 kDa using four activation methods: HCD, ETD, EThcD, and 193 nm UVPD. A set of six proteins was chosen to focus on ones with well-known sequences and allow significant signal averaging to increase the confidence in fragment ion assignments (in contrast to LCMS data acquisition, in which many proteins can be surveyed but with far lower sequence coverage and concomitant deterioration of confidence in ion assignments). We emphasize UVPD in particular owing to its high energy deposition and ability to cleave at every type of backbone position, generating six ion types (a/x, b/y, c/z) while preserving labile PTMs.[8,52] We compare performance metrics of the various activation methods, including sequence coverages, extent of preferential cleavages, and distribution of backbone cleavages throughout the sequence as a function of the charge state.

■ EXPERIMENTAL SECTION

Top-Down Mass Spectrometry. Ubiquitin (bovine, 8.6 kDa), cytochrome c (equine, 12.3 kDa), myoglobin (equine, 16.9 kDa), and carbonic anhydrase (bovine, 29.0 kDa) were obtained from Sigma-Aldrich. Staph nuclease (*Staphylococcus aureus*, 16.1 kDa)[53] and dihydrofolate reductase (*E. coli*, 18.9 kDa)[54] were expressed and produced as reported previously. Associated sequences, Uniprot accession numbers, and monoisotopic masses are listed in Table S1. LC−MS grade water, acetonitrile, and formic acid were obtained from Fischer Scientific. 4-Vinyl-1,3-dioxolan-2-one was obtained from Millipore Sigma. Each solution contained 5 μM protein in 1:1 water/acetonitrile with 0.1% v/v formic acid (denaturing conditions) and was infused by electrospray ionization using Pd/Au coated static tips (20 nm i.d.) pulled in-housed and using an applied voltage of 1.6 kV. Supercharged solutions also contained 1% v/v 4-vinyl-1,3-dioxolan-2-one. All spectra were collected using a Thermo Scientific Orbitrap Fusion Lumos Tribrid mass spectrometer, one equipped with a 213 nm solid state Nd:YAG laser (2 uJ per pulse, 2500 Hz repetition rate) and the other modified with a 500 Hz ArF excimer laser (Coherent, Inc.) for 193 nm UVPD as described earlier.[55] For the 193 nm UVPD, the laser power was adjusted to 1−2 mJ per pulse. Protein charge states were isolated using a 3 m/z isolation window. MS/MS spectra were acquired using a resolution of 240000, an AGC target of 1e6, an S-lens RF of

60%, 200 averages, and intact protein mode turned on. All data were collected in triplicate. Activation parameters for all methods and charge states were optimized for sequence coverage. Typical 213 nm UVPD used an activation period of 20−40 ms, corresponding to 50−100 laser pulses. Typical 193 nm UVPD parameters consisted of 1 laser pulse at 1−2 mJ per pulse. UVPD was performed in the low-pressure linear ion trap on both mass spectrometers. Activation parameters for HCD ranged from 4 to 25 NCE depending on the protein and charge state. Activation parameters for ETD ranged from 4 to 30 ms. For EThcD, a 4−30 ms period was used for ETD during which the HCD was between 5 and 23 NCE.

Data Analysis. All MS/MS spectra were deconvoluted using Xtract with a S/N threshold of 3 and a default fit factor of 44%, the latter based on the match between theoretical isotope distributions and experimental isotope distributions for each identified fragment ion. Fragments were identified using a 10 ppm error tolerance. Deconvoluted fragment ion abundances were analyzed with a custom-built Python program, MS-TAFI (https://github.com/kylejuetten), to generate fragment abundance maps.[56] All ten UVPD fragment ion types (*a*, *a*+1, *b*, *c*, *x*, *x*+1, *y*, *y*−1, *y*−2, and *z*) were considered for sequence coverage and general analysis of fragment abundances. When evaluating preferential cleavage sites, each inter-residue position is counted as one backbone cleavage site regardless of whether *a,b,c* or *x,y,z* ions are generated from cleavage of that inter-residue position. For percentages of fragment ion current originating from preferential backbone cleavages, all potential complementary partner ions (i.e., *a* and *x*, *b* and *y*, or *c* and *z*) are summed together if produced. All data is available in the public repository jPOST with the accession number JPST002123. Examples of MS/MS spectra are provided in Figures S1−S30.

RESULTS AND DISCUSSION

Charge-State Distributions. The charge-state distributions were evaluated for proteins sprayed from standard (50:50 water/acetonitrile, 0.1% v/v formic acid) and supercharging (50:50 water/acetonitrile, 0.1% v/v formic acid, 1% v/v 4-vinyl-1,3-dioxolan-2-one) solutions, both representing denaturing conditions. Examples of the MS1 spectra are shown in Figure 1 for cytochrome c (cytC) and carbonic anhydrase (CA), and the analogous MS1 spectra are shown in Figure S31 for the other four proteins included in this study. The charge-state distributions for the proteins sprayed under supercharging tended to narrow by 2 to 5 states depending on the protein size. The center of the charge state distribution also shifted by 2 to 5 charges on average. This effect generally varied with protein size, with proteins like cytochrome c showing large shifts in charge state distribution while proteins like carbonic anhydrase exhibiting less change (Figure 1). The charge states targeted for the detailed MS/MS analysis were selected to capture the widest range of charge states possible while still having sufficient signal (S/N > 50, typically corresponding to ≥5e5 normalized level for an Orbitrap Lumos mass spectrometer) for MS/MS experiments.

Sequence Coverage. Sequence coverage is often used as a metric for evaluating the impact of various parameters, whether experimental parameters or molecular features, on the fragmentation of a protein. The sequence coverages for proteins sprayed under standard and supercharging conditions were evaluated using HCD, ETD, EThcD, 213 nm UVPD, and 193 nm UVPD (Figure 2) for four charge states per protein

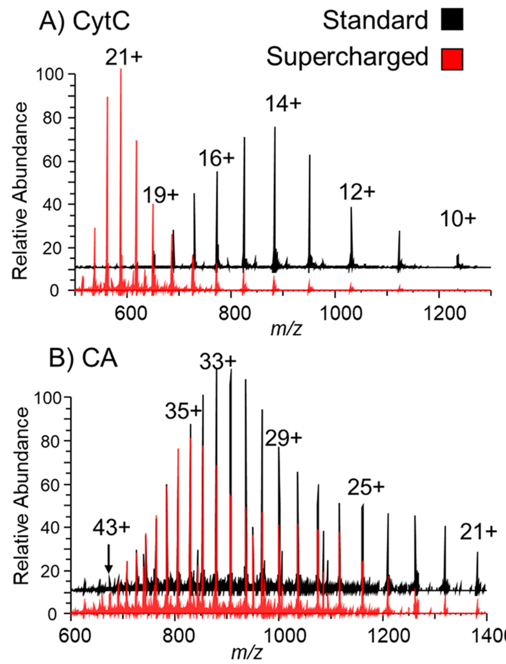

Figure 1. Charge-state distributions of (A) cytochrome c (CytC) and (B) carbonic anhydrase (CA) under standard (black) and supercharging (red) conditions.

(two standard charge states and two supercharged states). Representative sequence coverage maps are provided in Figures S32−S61. For all proteins analyzed, the sequence coverage acquired when using HCD tended to decrease as the charge state increased. The average decrease in sequence coverage for HCD going from the lowest to highest charge state was 23% for ubiquitin, 30% for cytochrome c, 41% for staph nuclease, 40% for myoglobin, 20% for dihydrofolate reductase, and 19% for carbonic anhydrase. This observation has been documented in previous studies which suggests that the decrease in sequence coverage for high charge states may be due to the abundance of a few key preferential fragmentation pathways such as those N-terminal to proline.[20−22] Combining this result with previous observations of proteins in low charge states activated by CID[12,13,20−22] suggests that "middle" charge states, neither the lowest nor highest, offer the best outcome for collisional activation of proteins. For low charge states, proton mobility is limited and cleavages at specific backbone sites are enhanced. At high charge states, the fragment ion current is also funneled toward key preferential sites.

When using ETD, the sequence coverage generally increased as the charge state increased, in agreement with the known dependence of the performance of electron activation methods on charge density.[57] The average increase for ETD on going from the lowest to highest charge state was 36% for ubiquitin, 11% for cytochrome c, 32% for staph nuclease, 10% for myoglobin, 26% for dihydrofolate reductase, and 9% for carbonic anhydrase. This outcome is consistent with the greater exothermicity of the electron-transfer reaction as a function of charge state of the precursor ion, increasing energy transfer and decreasing nondissociative processes.[57] In contrast to the more significant changes in sequence coverage as a function of charge state for HCD or ETD, there were minimal changes in sequence coverage for proteins activated using EThcD, 213 nm UVPD, and 193 nm UVPD. The change

https://doi.org/10.1021/jasms.3c00138
J. Am. Soc. Mass Spectrom. 2023, 34, 1467−1476

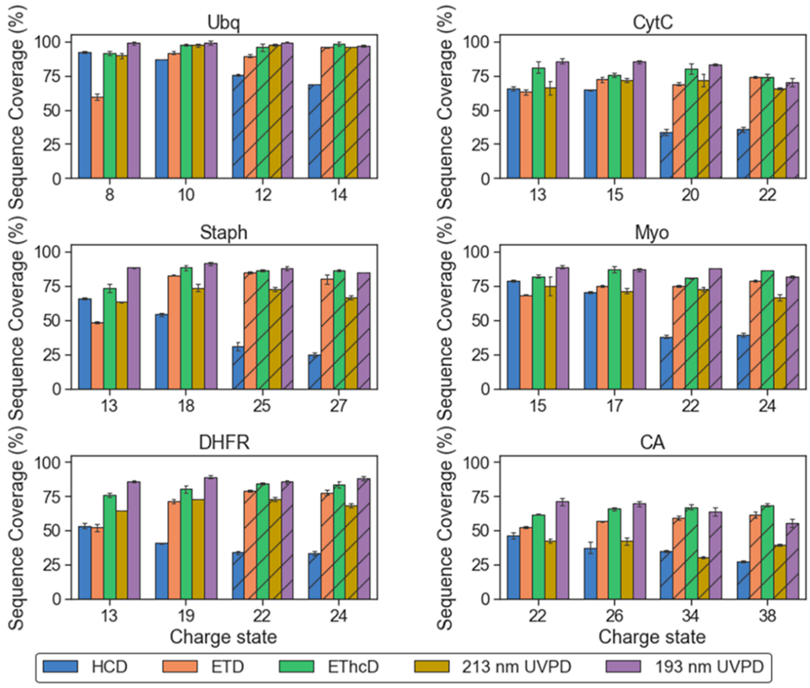

Figure 2. Summary of the sequence coverages obtained for ubiquitin (Ubq), cytochrome c (CytC), staph nuclease (Staph), myoglobin (Myo), dihydrofolate reductase (DHFR), and carbonic anhydrase (CA) across charge states using five activation methods. Hatched bars indicate supercharged states.

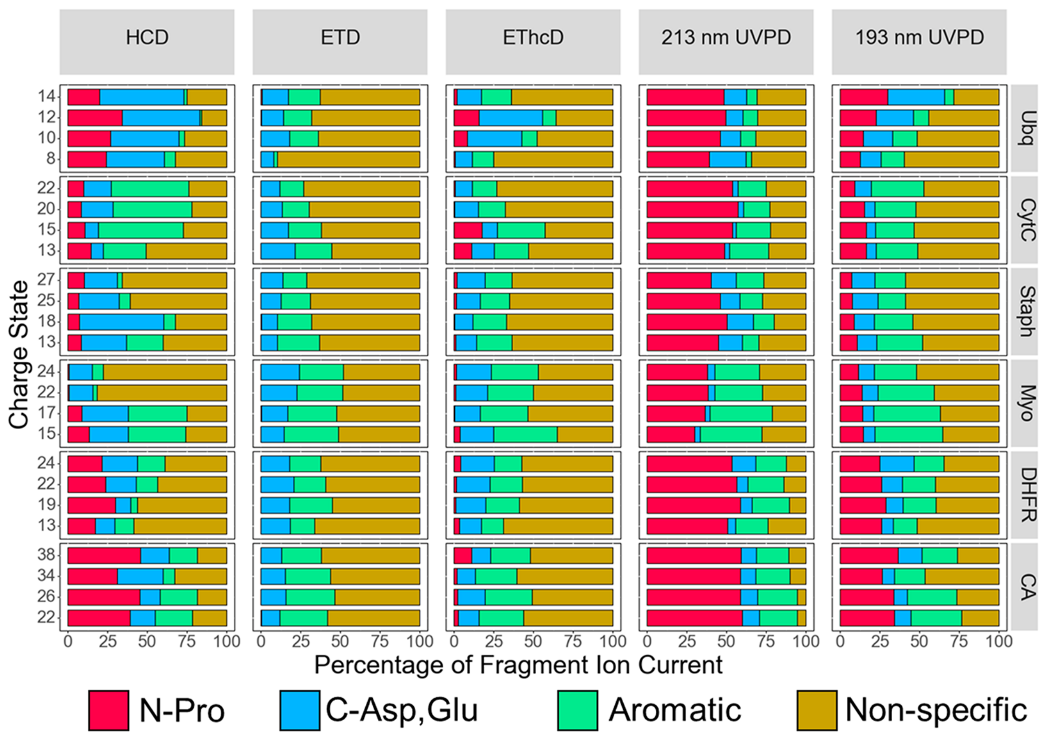

Figure 3. Percentages of ion current originating from preferential cleavages for (Ubq), cytochrome c (CytC), staph nuclease (Staph), myoglobin (Myo), dihydrofolate reductase (DHFR), and carbonic anhydrase (CA) for standard charge states and supercharged states for each activation method. Percentages are expressed as percentages of the total identified fragment ion current.

between the lowest and highest charge states when using any of these three activation methods ranged between 5 and 15%. The minimal changes in sequence coverage when using EThcD and UVPD have been documented in past studies which have examined the impact of charge state.[32,35]

One additional metric related to sequence coverage is the concept of reciprocal ions. Reciprocal fragment ions are those that originate from cleavages of the same backbone position and thus map the same backbone site. These are counted by assigning the most abundant fragment originating from each backbone position as unique, with all other fragments at that

https://doi.org/10.1021/jasms.3c00138
J. Am. Soc. Mass Spectrom. 2023, 34, 1467−1476

same position categorized as reciprocal. The downside of reciprocal ions is that they map the same backbone position, but the benefit is that they provide additional opportunities to map a position that might otherwise be missed if one relies solely on one type of fragment ion. This reciprocal fragment ion analysis is shown in Figure S62 for all six proteins. As expected, 193 nm UVPD yielded the highest reciprocal values (most reciprocal fragment ions), followed by 213 nm UVPD or EThcD, ETD, and HCD. This trend held regardless of the charge state.

Preferential Cleavages. The effect of supercharging agents on the extent of preferential cleavages was explored. In particular, the preferential cleavages of interest include backbone cleavages N-terminal to proline (Pro,P) residues, C-terminal to acidic residues (aspartate (Asp,D), glutamate (Glu,E)), and cleavages adjacent to aromatic residues ((Phe, F), (Tyr, Y), and (Trp, W)), the latter of which are more commonly noted for UVPD methods. For each protein and charge state, the number (count) and abundances of all fragment ions were pooled and then categorized based on the locations of the backbone cleavages from which the fragment ions originated.

Backbone Cleavage N-Terminal to Proline (Pro). The most notable finding with respect to the preferential N-terminal proline cleavage for supercharged proteins is the significant enhancement of this pathway for 213 nm UVPD relative to all other activation methods, in agreement with prior studies of proteins in standard charge states which highlighted the dominance of this pathway for 213 nm UVPD.[34,35] For proteins activated using HCD, the percentage of total fragment ion current and number of fragment ions attributed to backbone cleavage N-terminal to proline generally remained unchanged or slightly decreased for supercharged ions (Figures 3, S62, and S63). The impacts of supercharging on N-terminal proline cleavage for both ETD and EThcD were negligible as these activation methods do not promote this fragmentation pathway (Figures 3 and S64−S67).[58] For 213 and 193 nm UVPD, the trend in N-terminal proline cleavage as a percentage of the total ion current did not show a consistent outcome as a function of protein charge state, increasing for one of the supercharged proteins (cytC) but decreasing for DHFR or showing little change for the other proteins. The same number of proline cleavages occurred for all charge states of each protein for 213 nm UVPD (Figures 3 and Figures S68−S69), also echoed for 193 nm UVPD (Figures 3, S70, and S71). In general, the portion of fragment ion current attributed to proline-mediated cleavage varied significantly based on the activation method and varied moderately based on charge state.

Backbone Cleavage C-Terminal to Acidic Residue (Asp, Glu). For collisional activation of peptides, the mobile proton model suggests that acidic cleavages are favored when the number of added protons is less than the number of basic residues along the protein backbone (i.e., limited proton mobility).[16] This finding has also been substantiated for collisional activation of proteins.[13,20−22,26] In the present study, for HCD there is a consistent decrease in the number of fragment ions originating from cleavages C-terminal to acidic residues for the supercharged proteins. (Figure S62). When expressing this value as a percentage of the total number of possible cleavages C-terminal to acidic residues, the decrease for each protein is 10% for ubiquitin, 33% for cytochrome c, 50% for staph nuclease, 43% for myoglobin, 30% for dihydrofolate reductase, and 24% for carbonic anhydrase when going from the lowest to highest charge states analyzed (Figure S63). For ETD, EThcD, 213 nm UVPD, and 193 nm UVPD, the total number of identified acidic cleavages and abundances of the resulting ions remained nearly constant across all charge states (Figures S64−S71). Comparison of the patterns for the five activation methods indicates that backbone cleavages C-terminal to acidic residues contribute a significantly greater portion of the fragment ions for HCD than any of the other methods. This result is not unexpected given the dependence of this fragmentation pathway on the charge state and number of mobile protons, and it is also consistent with the prevailing perspective that the outcome of UVPD is not significantly influenced by the charge state. To summarize, only HCD showed a consistent decrease in the number of C-terminal cleavages to acidic residues under supercharging conditions, whereas ETD, EThcD, and UVPD showed minimal changes with increasing charge state.

Backbone Cleavages Adjacent to Aromatic Residues (Phe, Tyr, Trp). The number and total portion of product ions originating from cleavages adjacent to aromatic residues (Phe, Tyr, Trp) were also monitored for all activation methods (Figures 3 and S62−S71). Enhancement of fragmentation adjacent to aromatic residues has been reported previously for UVPD of proteins,[12] but this effect has not been recognized as a notable factor for other activation methods. While 213 and 193 nm UVPD both yielded a greater number of fragment ions originating from aromatic cleavages compared to other activation methods (Figures S68 and S70), the percentage of the total ion current contributing to these ions was similar or in some cases lower than observed for the other activation methods (Figure 3). These results indicate that while aromatic cleavages may occur more frequently for UVPD, they do not necessarily result in highly abundant fragment ions. This observation appears to be largely independent of charge state as the number and abundances of products arising from cleavages adjacent to aromatic residues varied depending on the protein, activation method, and charge state.

Nonspecific Backbone Cleavages. The bulk of fragment ions originate from backbone cleavages at positions unrelated to the presence of proline, acidic, or aromatic residues, and these are collectively grouped as products from nonspecific cleavages. Nonspecific cleavages were dominant for both ETD and EThcD regardless of charge state. 213 nm UVPD and 193 nm UVPD showed minimal changes in the number of fragment ions arising from nonspecific cleavage as a function of charge state, although 193 nm UVPD consistently resulted in a larger number of nonspecific cleavages than 213 nm UVPD. Only with HCD did the number of nonspecific cleavages consistently decrease with increasing charge, but the total ion current from such products did not. For HCD, the number of fragment ions originating from nonspecific cleavages decreased for all proteins in supercharged states; however, their contribution to the total fragment ion current varied and showed a decrease for ubiquitin, cytochrome c, and dihydrofolate reductase and an increase for staph nuclease and myoglobin. Little effect was observed for carbonic anhydrase (Figures 3 and S62−S71). This outcome parallels the trends discussed previously for HCD as the sequence coverage tended to decrease with increasing charge state, while the number of identified preferential cleavages remained constant.

Overall Percentages of Preferential and Nonspecific Fragment Ions. To examine the overall differences in the

https://doi.org/10.1021/jasms.3c00138
J. Am. Soc. Mass Spectrom. 2023, 34, 1467−1476

portion of fragment ions originating from preferential versus nonspecific cleavage, all fragment ions attributed to preferential (N-Pro, C-Asp + Glu, aromatic) cleavages were grouped together and their abundances summed and compared to the portion arising from nonspecific cleavages (Figure S72). For HCD, the portion of fragment ions from preferential cleavages increased relative to the portion from nonspecific cleavage for ubiquitin, cytochrome c, and dihydrofolate reductase for the supercharged states. Product ions from nonspecific cleavages were more abundant for staph nuclease and myoglobin for the supercharged states. This result can be seen in the fragment abundance maps for these two proteins, which show the emergence of highly abundant fragment ions originating from Q/G and A/D backbone cleavages for myoglobin (22+, 24+) and staph nuclease (25+, 27+), respectively (Figures S87 and S88). For ETD, EThcD, 213 nm UVPD, and 193 nm UVPD, the proportion of fragment ion current originating from preferential versus nonspecific cleavages remained relatively constant for each protein in standard versus supercharged states (Figure S72). However, it is notable that the overall proportion of product ions from preferential cleavages is significantly greater than the portion from nonspecific cleavages for all proteins and all charge states for 213 nm UVPD.

Other Trends Related to Activation Method. Broader trends related to the total number of identified fragments were also considered, as this accounts for the entire set of fragment ions that contribute to the sequence coverage (in contrast to the counting of backbone cleavage sites). This metric differs from the ones discussed previously because it tallies all fragment ions (e.g., *a*, *a*+1, *b*, *c*, *x*, *x*+1, *y*, *y*−1, *y*−2, and *z*) regardless of whether they contribute new information or originate from different backbone positions (such as b_{36} and c_{36} ions). All six proteins followed a similar trend regardless of the charge state (Figure S73). 193 nm UVPD consistently generated the greatest number of fragment ions, followed by EThcD, 213 nm UVPD, and either HCD or ETD. HCD produced more fragments for low charge states, whereas ETD produced more fragments for high charge states. For four of the proteins (Ubq, CytC, Myo, and DHFR), it appears that there are more C-terminal fragment ions than N-terminal ions produced, but it seems that N-terminal fragment ions are favored for CA (Figures S74 and S75). To explore these trends in more detail, the variation and distribution of specific ion types were further analyzed and summarized in Figures S76−S80 for each activation method. Ion types were grouped according to their broader families (i.e., *a*, *a*+1 grouped together; and *y*, *y*−1, *y*−2 all grouped as *y*-type). For 213 nm UVPD, *a*, *x*, and *y* ions were most dominant for all proteins, whereas 193 nm UVPD resulted in a broader distribution of all six ion types.

The MS/MS spectra were also scrutinized to discern whether supercharging resulted in the identification of unique backbone cleavage sites (Table 1; Figures S81−S85). As an example, for analysis of DHFR the number of unique cleavage sites (3) produced by HCD of the supercharged states (22+, 24+) is significantly lower than the number of unique cleavage sites (43) generated by HCD of the standard charge states, indicating a substantial decrease in the sequence information. For ETD and both 213 and 193 nm UVPD of DHFR (Table 1), supercharging led to production of several more unique backbone cleavage sites than obtained for the standard charge states. For HCD in general, supercharging appears to

Table 1. Summary of Unique or Shared Backbone Cleavages for Dihydrofolate Reductase (DHFR) for Standard Charge States (13+, 19+) or Supercharged States (22+, 24+)

DHFR	Unique Backbone Cleavages Standard (13+, 19+)	Shared Backbone Cleavages	Unique Backbone Cleavages Supercharged (22+, 24+)
HCD	43	56	3
ETD	4	122	19
EThcD	9	139	11
213 nm UVPD	9	139	11
193 nm UVPD	9	118	10

streamline fragmentation pathways as there are few unique cleavage sites for all of the proteins in higher charge states, and most of the identified backbone cleavages for the supercharged states are shared with the standard charge states (Figure S81). Conversely, the ETD of the supercharged states consistently led to the greatest number of new backbone cleavage sites, averaging 18 new backbone cleavages across all six proteins (Figure S82). Supercharging resulted in an average of 9 new backbone cleavage sites for EThcD, 11 for 213 nm UVPD, and only 6 for 193 nm UVPD (Figures S83−S85). The relatively low gain for 193 nm UVPD is attributed to the high sequence coverage obtained for the standard charge states, leaving little room for improvement for higher charge states.

■ BACKBONE CLEAVAGE MAPS

To further examine the impacts of supercharging on preferential cleavages, backbone cleavage maps were created using a Python program, MS-TAFI.[56] This program utilizes deconvoluted fragment ion abundances to display the abundances of fragments (normalized to the total fragment ion current) according to the backbone cleavage position from which they originated, allowing visualization of the pattern of backbone cleavages ("cut sites") throughout the protein sequence. This format graphically illustrates the impact of highly preferred cleavage sites as a function of charge state and also improves visualization of variations in coverage of the protein sequence for each activation method. These backbone cleavage maps were created for each protein and each charge state for each activation method, as illustrated in Figures 4 for ubiquitin and S86−S90 for the other five proteins.

The backbone cleavage maps reveal some notable shifts in the fragmentation patterns for most of the proteins for the standard versus supercharged states. The backbone cleavage maps generated for the HCD spectra indicate that much of the ion current is funneled into a few fragment ions originating from specific backbone cleavage sites, commonly related to Pro, Asp, or Glu cleavages, features that are even more pronounced for higher charge states. For example, a b_{18} ion is prominent for all charge states of ubiquitin, and this ion arises from a backbone cleavage (E/P) that is both C-terminal to an acidic residue and N-terminal to proline, which have previously been defined as preferential pathways. Supercharging in this case accentuates this particular preferential cleavage site. The observation of enhanced preferential cleavages upon HCD, particularly for the supercharged states, is echoed in the backbone cleavage maps generated for the other proteins. The trend for enhancement of preferential backbone cleavage sites is reversed for ETD. Some cleavages that are prominently favored for the lower charge states, such as a G/K cleavage that

https://doi.org/10.1021/jasms.3c00138
J. Am. Soc. Mass Spectrom. 2023, 34, 1467−1476

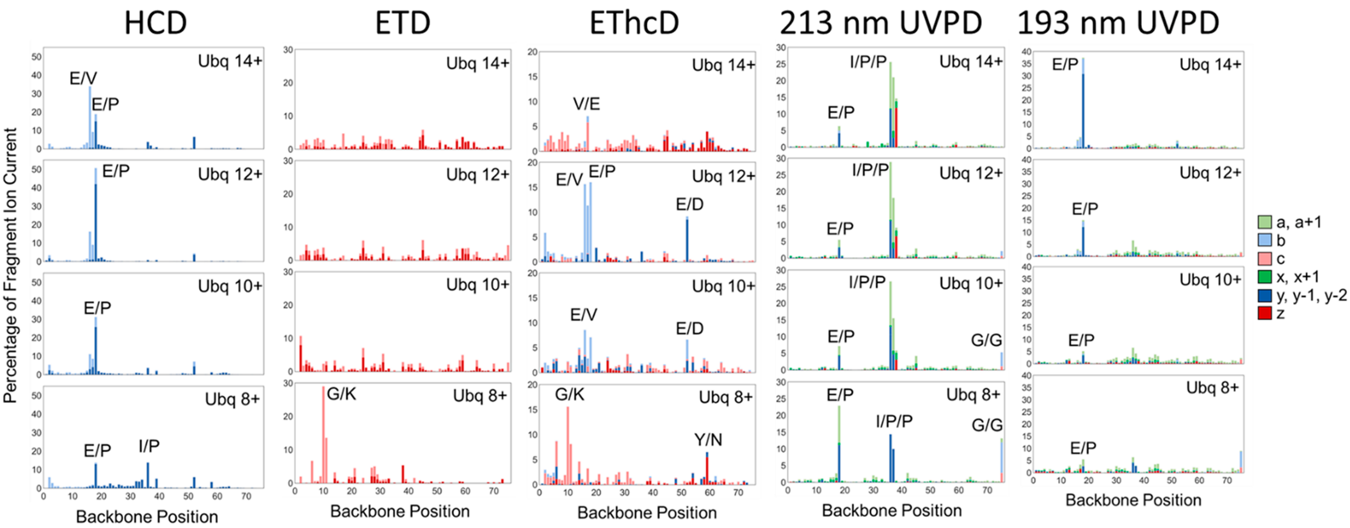

Figure 4. Backbone cleavage maps based on fragment ions originating from backbone cleavages throughout the sequence of ubiquitin (Ubq) for standard charge states (8+, 10+) and supercharged states (12+, 14+) activated using HCD, ETD, EThcD, 213 nm UVPD, and 193 nm UVPD. Fragments are color coded according to ion type, and abundances are displayed as a percentage of the total identified fragment ion current. Hydrogen shift fragment ions (e.g., a+1, x+1, y−1, and y−2) are included for spectra generated by UVPD.

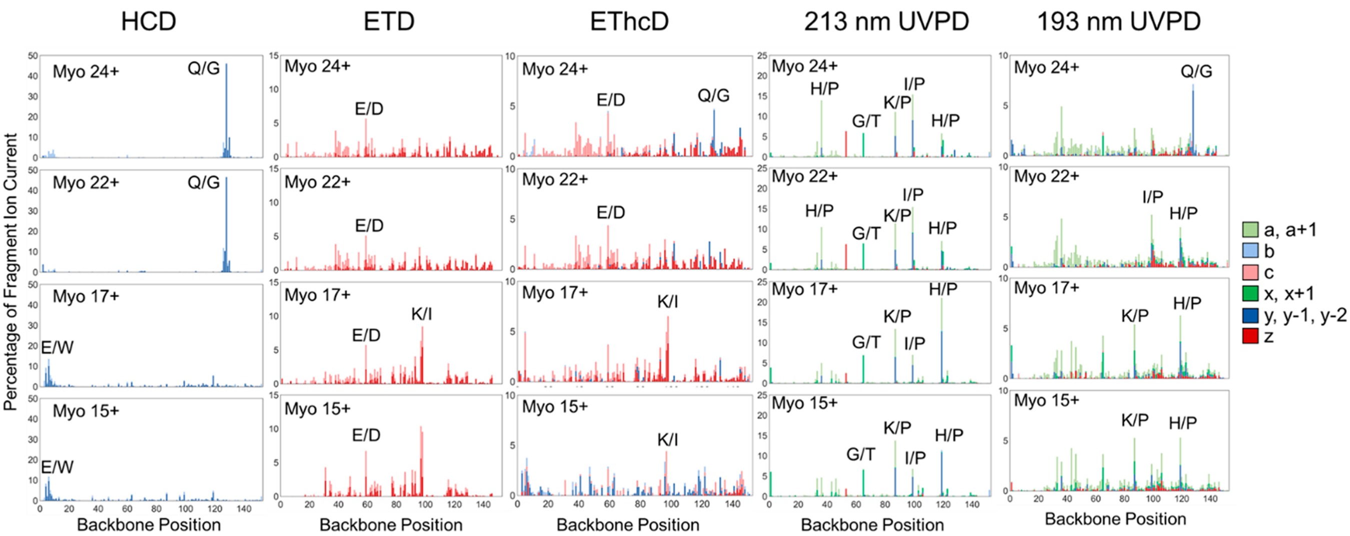

Figure 5. Backbone cleavage maps based on fragment ions originating from backbone cleavages throughout the sequence of myoglobin (Myo) for standard charge states (15+, 17+) and supercharged states (22+, 24+) activated using HCD, ETD, EThcD, 213 nm UVPD, and 193 nm UVPD. Fragments are color coded according to ion type, and abundances are displayed as a percentage of the total identified fragment ion current. Hydrogen shift fragment ions (e.g., a+1, x+1, y−1, y−2) are included for spectra generated by UVPD.

results in a highly abundant c_{10} ion for ubiquitin (8+) (Figure 4), diminish in prevalence for the higher charge states, along with production of a broader array of fragment ions. EThcD exhibits backbone cleavage patterns that blend the trends noted for HCD and ETD, with some prominent preferential backbone cleavages emerging for the supercharged states, but in general a more heterogeneous array of backbone cleavages for all charge states. Some of the dominant backbone cleavage sites shift significantly, as observed in the backbone cleavage maps for ubiquitin in Figure 4 in which ETD-type z ions originating from G/K and Y/N cleavages are prominent for the 8+ charge state, HCD-type b ions arising from E/V and E/D cleavages are most abundant for the 10+ and 12+ charge states, and then a z ion from a V/E backbone cleavage is favored for the 14+ charge state. For both ETD and EThcD, the production of highly abundant fragment ions from a few specific backbone cleavage sites is balanced by a broad array of other lower abundance fragment ions through the cleavage of other backbone sites.

The backbone cleavage maps for both 213 and 193 nm UVPD data also reveal interesting observations. While the sequence coverage does not vary much according to charge state for ubiquitin, there is a significant funneling of ion current into a handful of fragment ions from preferential backbone cleavage sites (E/P, P/P) as protein charge state increases (Figure 4). In addition, the fragment ions that originate from these cleavage sites are often b/y-type ions commonly associated with collisional activation type fragmentation. A previous CID study of ubiquitin reported changes in preferential cleavages from low (2+) to high (12+) charge states, specifically noting a shift in the degree of cleavages adjacent to acidic residues for low charge states to those mediated by proline residues for high charge states.[20] This invites speculation about the location of charges and how this influences fragmentation for UVPD. One fragment ion that is the most abundant fragment ion for 193 nm UVPD of supercharged myoglobin (24+) is a y_{25} ion related to a Q/G backbone cleavage, also observed for HCD (Figure 5), bolstering the idea that this pathway is occurring through a mechanism that is more akin to the processes occurring for collisional activated dissociation and not a direct pathway from an excited electronic state. When comparing the fragmentation trends for 213 and 193 nm UVPD, a similar trend is observed where ion current is funneled toward specific backbone cleavages, although this effect is more pronounced for 213 nm UVPD. While N-terminal proline cleavage is prominent across all charge states, certain sites appear to be enhanced for supercharged states. For 213 nm UVPD, cytochrome c exhibits enhanced cleavage an I/P site for the supercharged states, a cleavage site that was less pronounced for standard charge states. This finding holds true for a Q/P cleavage site for staph nuclease as well. These cleavages are also pronounced for 193 nm UVPD contributions, and all are related to the production of *b*/*y*-type ions.

One other factor that should be considered when deciphering the enhancement of certain fragmentation pathways is the potential changes in the protein structure upon supercharging. While a protein is denatured in both standard and supercharged solutions (containing 1:1 water/acetonitrile with 0.1% v/v formic acid), the ensemble of structures may be different and potentially result in a distribution of elongated versus collapsed structures. Some of this variation may be reflected in a protein's collision cross-section, which measures an ion's size. Higher charge states typically present larger collision cross sections, especially from denaturing solutions. The change in collision cross section when going from standard charge states to supercharged states can be quite large, in some cases ranging from 23 to 36%.[59] For example, the collision cross-section of ubiquitin increased from 1990 Å^2 (8+) to 2600 Å^2 (13+), and similar increases were noted for myoglobin (3880 Å^2 (15+) to 5090 Å^2 (24+)) and carbonic anhydrase (5959 Å^2 (22+) to 8142 Å^2 (33+)).[59] It is reasonable to postulate that a change in protein structure, e.g., even more protein elongation owing to Coulombic repulsion from supercharging, may also contribute to changes in fragmentation.

CONCLUSION

The effects of supercharging on the fragmentation of denatured proteins were investigated using a variety of activation methods. Some increases in sequence coverage with increasing charge state were observed for ETD; however, significant decreases were observed for HCD. In contrast, EThcD, 213 nm UVPD, and 193 nm UVPD showed relatively minimal changes in sequence coverage for supercharged states while also offering the consistently highest average sequence coverage among the activation methods. The decrease in sequence coverage observed for HCD of supercharged denatured proteins contrasts with the increase in sequence coverage reported for CID of supercharged native-like protein complexes for which significant enhancement of product ions was observed, an outcome attributed to the higher dissociation efficiencies of the higher charge states.[40] Native-like proteins typically have very low charge states, and the addition of extra protons shifts the charge states to ones more amenable to CID and does not reach the same high charge regime of supercharged denatured proteins.

Supercharging influenced the number and abundances of fragment ions originating from preferential backbone cleavages (N-terminal proline and C-terminal aspartic acid/glutamic acid) depending on the activation method. Particularly for HCD, 213 nm UVPD, and 193 nm UVPD, often a few backbone cleavage sites were increasingly favored for the supercharged states. Furthermore, the fragment ions that originated from preferential backbone cleavage sites upon 213 or 193 nm UVPD of supercharged states were frequently *b*/*y*-type ions that are commonly associated with the pathways favored for collisional activation. Overall, the variations in fragmentation of proteins as a function of charge state suggest that optimization of the charge state and combining results from several charge states may maximize sequence coverage based on modulation of the preferred backbone cleavage sites and fragment ion abundances.

ASSOCIATED CONTENT

Supporting Information

The Supporting Information is available free of charge at https://pubs.acs.org/doi/10.1021/jasms.3c00138.

Tables summarizing the protein sequences, representative MS/MS spectra for all proteins and activation methods, sequence coverage maps, additional figures displaying preferential cleavage abundances, Venn diagrams displaying unique cleavage sites, and fragment abundance maps (PDF)

AUTHOR INFORMATION

Corresponding Author

Jennifer S. Brodbelt − *Department of Chemistry, University of Texas at Austin, Austin, Texas 78712, United States;* orcid.org/0000-0003-3207-0217; Email: jbrodbelt@cm.utexas.edu

Author

Kyle J. Juetten − *Department of Chemistry, University of Texas at Austin, Austin, Texas 78712, United States*

Complete contact information is available at: https://pubs.acs.org/10.1021/jasms.3c00138

Notes

The authors declare no competing financial interest.

ACKNOWLEDGMENTS

Funding from NSF (CHE-2203602), the Robert A. Welch Foundation (F-1155), and the UT System for support of the UT System Proteomics Core Facility Network is gratefully acknowledged.

REFERENCES

(1) McLafferty, F. W.; Breuker, K.; Jin, M.; Han, X.; Infusini, G.; Jiang, H.; Kong, X.; Begley, T. P. Top-down MS, a Powerful Complement to the High Capabilities of Proteolysis Proteomics. *FEBS Journal* **2007**, *274* (24), 6256−6268.

(2) Catherman, A. D.; Skinner, O. S.; Kelleher, N. L. Top Down Proteomics: Facts and Perspectives. *Biochem. Biophys. Res. Commun.* **2014**, *445* (4), 683−693.

(3) Zhang, H.; Ge, Y. Comprehensive Analysis of Protein Modifications by Top-Down Mass Spectrometry. *Circ Cardiovasc Genet* **2011**, *4* (6), 711−711.

(4) Zhang, Y.; Fonslow, B. R.; Shan, B.; Baek, M.-C.; Yates, J. R. I. Protein Analysis by Shotgun/Bottom-up Proteomics. *Chem. Rev.* **2013**, *113* (4), 2343−2394.

(5) Han, X.; Aslanian, A.; Yates, J. R. Mass Spectrometry for Proteomics. *Curr. Opin. Chem. Biol.* **2008**, *12* (5), 483−490.

(6) Macias, L. A.; Santos, I. C.; Brodbelt, J. S. Ion Activation Methods for Peptides and Proteins. *Anal. Chem.* **2020**, *92* (1), 227−251.

(7) Zhurov, K. O.; Fornelli, L.; Wodrich, M. D.; Laskay, Ü. A.; Tsybin, Y. O. Principles of Electron Capture and Transfer Dissociation Mass Spectrometry Applied to Peptide and Protein Structure Analysis. *Chem. Soc. Rev.* **2013**, *42* (12), 5014−5030.

(8) Brodbelt, J. S.; Morrison, L. J.; Santos, I. Ultraviolet Photodissociation Mass Spectrometry for Analysis of Biological Molecules. *Chem. Rev.* **2020**, *120* (7), 3328−3380.

(9) Toby, T. K.; Fornelli, L.; Kelleher, N. L. Progress in Top-Down Proteomics and the Analysis of Proteoforms. *Annual Rev. Anal. Chem.* **2016**, *9* (1), 499−519.

(10) Siuti, N.; Kelleher, N. L. Decoding Protein Modifications Using Top-down Mass Spectrometry. *Nat. Methods* **2007**, *4* (10), 817−821.

(11) Cui, W.; Rohrs, H. W.; Gross, M. L. Top-down Mass Spectrometry: Recent Developments, Applications and Perspectives. *Analyst* **2011**, *136* (19), 3854.

(12) Bashyal, A.; Sanders, J. D.; Holden, D. D.; Brodbelt, J. S. Top-Down Analysis of Proteins in Low Charge States. *J. Am. Soc. Mass Spectrom.* **2019**, *30* (4), 704−717.

(13) Cobb, J. S.; Easterling, M. L.; Agar, J. N. Structural Characterization of Intact Proteins Is Enhanced by Prevalent Fragmentation Pathways Rarely Observed for Peptides. *J. Am. Soc. Mass Spectrom.* **2010**, *21* (6), 949−959.

(14) Syka, J. E. P.; Coon, J. J.; Schroeder, M. J.; Shabanowitz, J.; Hunt, D. F. Peptide and Protein Sequence Analysis by Electron Transfer Dissociation Mass Spectrometry. *Proc. Natl. Acad. Sci. U. S. A.* **2004**, *101* (26), 9528−9533.

(15) Macias, L. A.; Sipe, S. N.; Santos, I. C.; Bashyal, A.; Mehaffey, M. R.; Brodbelt, J. S. Influence of Primary Structure on Fragmentation of Native-Like Proteins by Ultraviolet Photodissociation. *J. Am. Soc. Mass Spectrom.* **2021**, *32* (12), 2860−2873.

(16) Wysocki, V. H.; Tsaprailis, G.; Smith, L. L.; Breci, L. A. Mobile and Localized Protons: A Framework for Understanding Peptide Dissociation. *J. Mass Spectrom.* **2000**, *35*, 1399−1406.

(17) Bythell, B. J.; Suhai, S.; Somogyi, A.; Paizs, B. Proton-Driven Amide Bond-Cleavage Pathways of Gas-Phase Peptide Ions Lacking Mobile Protons. *J. Am. Chem. Soc.* **2009**, *131* (39), 14057−14065.

(18) Dongré, A. R.; Jones, J. L.; Somogyi, A.; Wysocki, V. H. Influence of Peptide Composition, Gas-Phase Basicity, and Chemical Modification on Fragmentation Efficiency: Evidence for the Mobile Proton Model. *J. Am. Chem. Soc.* **1996**, *118* (35), 8365−8374.

(19) Konermann, L.; Aliyari, E.; Lee, J. H. Mobile Protons Limit the Stability of Salt Bridges in the Gas Phase: Implications for the Structures of Electrosprayed Protein Ions. *J. Phys. Chem. B* **2021**, *125* (15), 3803−3814.

(20) Reid, G. E.; Wu, J.; Chrisman, P. A.; Wells, J. M.; McLuckey, S. A. Charge-State-Dependent Sequence Analysis of Protonated Ubiquitin Ions via Ion Trap Tandem Mass Spectrometry. *Anal. Chem.* **2001**, *73* (14), 3274−3281.

(21) Newton, K. A; Chrisman, P. A; Reid, G. E; Wells, J.M.; McLuckey, S. A Graham Cooks on the Occasion of His 60th Birthday. *Int. J. Mass Spectrom.* **2001**, *212* (1), 359−376.

(22) Chanthamontri, C.; Liu, J.; McLuckey, S. A. Charge State Dependent Fragmentation of Gaseous α-Synuclein Cations via Ion Trap and Beam-Type Collisional Activation. *Int. J. Mass Spectrom.* **2009**, *283* (1−3), 9−16.

(23) Pitteri, S. J.; Reid, G. E.; McLuckey, S. A. Affecting Proton Mobility in Activated Peptide and Whole Protein Ions via Lysine Guanidination. *J. Proteome Res.* **2004**, *3* (1), 46−54.

(24) Haverland, N. A.; Skinner, O. S.; Fellers, R. T.; Tariq, A. A.; Early, B. P.; LeDuc, R. D.; Fornelli, L.; Compton, P. D.; Kelleher, N. L. Defining Gas-Phase Fragmentation Propensities of Intact Proteins During Native Top-Down Mass Spectrometry. *J. Am. Soc. Mass Spectrom.* **2017**, *28* (6), 1203−1215.

(25) Ives, A. N.; Su, T.; Durbin, K. R.; Early, B. P.; dos Santos Seckler, H.; Fellers, R. T.; LeDuc, R. D.; Schachner, L. F.; Patrie, S. M.; Kelleher, N. L. Using 10,000 Fragment Ions to Inform Scoring in Native Top-down Proteomics. *J. Am. Soc. Mass Spectrom.* **2020**, *31* (7), 1398−1409.

(26) Foreman, D. J.; Dziekonski, E. T.; McLuckey, S. A. Maximizing Selective Cleavages at Aspartic Acid and Proline Residues for the Identification of Intact Proteins. *J. Am. Soc. Mass Spectrom.* **2019**, *30* (1), 34−44.

(27) Zubarev, R. A.; Horn, D. M.; Fridriksson, E. K.; Kelleher, N. L.; Kruger, N. A.; Lewis, M. A.; Carpenter, B. K.; McLafferty, F. W. Electron Capture Dissociation for Structural Characterization of Multiply Charged Protein Cations. *Anal. Chem.* **2000**, *72* (3), 563−573.

(28) Riley, N. M.; Westphall, M. S.; Coon, J. J. Activated Ion Electron Transfer Dissociation for Improved Fragmentation of Intact Proteins. *Anal. Chem.* **2015**, *87* (14), 7109−7116.

(29) Riley, N. M.; Westphall, M. S.; Coon, J. J. Activated Ion-Electron Transfer Dissociation Enables Comprehensive Top-Down Protein Fragmentation. *J. Proteome Res.* **2017**, *16* (7), 2653−2659.

(30) Swaney, D. L.; McAlister, G. C.; Wirtala, M.; Schwartz, J. C.; Syka, J. E. P.; Coon, J. J. Supplemental Activation Method for High-Efficiency Electron-Transfer Dissociation of Doubly Protonated Peptide Precursors. *Anal. Chem.* **2007**, *79* (2), 477−485.

(31) Coon, J. J. Collisions or Electrons? Protein Sequence Analysis in the 21st Century. *Anal. Chem.* **2009**, *81* (9), 3208−3215.

(32) Riley, N. M.; Westphall, M. S.; Coon, J. J. Sequencing Larger Intact Proteins (30−70 KDa) with Activated Ion Electron Transfer Dissociation. *J. Am. Soc. Mass Spectrom.* **2018**, *29* (1), 140−149.

(33) Greer, S. M.; Holden, D. D.; Fellers, R.; Kelleher, N. L.; Brodbelt, J. S. Modulation of Protein Fragmentation Through Carbamylation of Primary Amines. *J. Am. Soc. Mass Spectrom.* **2017**, *28* (8), 1587−1599.

(34) Fornelli, L.; Srzentić, K.; Toby, T. K.; Doubleday, P. F.; Huguet, R.; Mullen, C.; Melani, R. D.; dos Santos Seckler, H.; DeHart, C. J.; Weisbrod, C. R.; Durbin, K. R.; Greer, J. B.; Early, B. P.; Fellers, R. T.; Zabrouskov, V.; Thomas, P. M.; Compton, P. D.; Kelleher, N. L. Thorough Performance Evaluation of 213 Nm Ultraviolet Photodissociation for Top-down Proteomics*. *Molecular & Cellular Proteomics* **2020**, *19* (2), 405−420.

(35) Lanzillotti, M.; Brodbelt, J. S. Comparison of Top-Down Protein Fragmentation Induced by 213 and 193 Nm UVPD. *J. Am. Soc. Mass Spectrom.* **2023**, *34*, 279.

(36) Lomeli, S. H.; Peng, I. X.; Yin, S.; Ogorzalek Loo, R. R.; Loo, J. A. New Reagents for Increasing ESI Multiple Charging of Proteins and Protein Complexes. *J. Am. Soc. Mass Spectrom.* **2010**, *21* (1), 127.

(37) Hopper, J. T. S.; Sokratous, K.; Oldham, N. J. Charge State and Adduct Reduction in Electrospray Ionization-Mass Spectrometry Using Solvent Vapor Exposure. *Anal. Biochem.* **2012**, *421* (2), 788−790.

(38) Laszlo, K. J.; Munger, E. B.; Bush, M. F. Folding of Protein Ions in the Gas Phase after Cation-to-Anion Proton-Transfer Reactions. *J. Am. Chem. Soc.* **2016**, *138* (30), 9581−9588.

(39) Foreman, D. J.; McLuckey, S. A. Recent Developments in Gas-Phase Ion/Ion Reactions for Analytical Mass Spectrometry. *Anal. Chem.* **2020**, *92* (1), 252−266.

(40) Yin, S.; Loo, J. A. Top-down Mass Spectrometry of Supercharged Native Protein-Ligand Complexes. *Int. J. Mass Spectrom.* **2011**, *300* (2), 118−122.

(41) Teo, C. A.; Donald, W. A. Solution Additives for Supercharging Proteins beyond the Theoretical Maximum Proton-Transfer Limit in Electrospray Ionization Mass Spectrometry. *Anal. Chem.* **2014**, *86* (9), 4455−4462.

(42) Going, C. C.; Xia, Z.; Williams, E. R. New Supercharging Reagents Produce Highly Charged Protein Ions in Native Mass Spectrometry. *Analyst* **2015**, *140* (21), 7184−7194.

(43) Iavarone, A. T.; Jurchen, J. C.; Williams, E. R. Supercharged Protein and Peptide Ions Formed by Electrospray Ionization. *Anal. Chem.* **2001**, *73* (7), 1455−1460.
(44) Zenaidee, M. A.; Donald, W. A. Extremely Supercharged Proteins in Mass Spectrometry: Profiling the PH of Electrospray Generated Droplets, Narrowing Charge State Distributions, and Increasing Ion Fragmentation. *Analyst* **2015**, *140* (6), 1894−1905.
(45) Metwally, H.; McAllister, R. G.; Popa, V.; Konermann, L. Mechanism of Protein Supercharging by Sulfolane and *m* -Nitrobenzyl Alcohol: Molecular Dynamics Simulations of the Electrospray Process. *Anal. Chem.* **2016**, *88* (10), 5345−5354.
(46) Yao, Y.; Richards, M. R.; Kitova, E. N.; Klassen, J. S. Influence of Sulfolane on ESI-MS Measurements of Protein-Ligand Affinities. *J. Am. Soc. Mass Spectrom.* **2016**, *27* (3), 498−506.
(47) Martin, L. M.; Konermann, L. Sulfolane-Induced Supercharging of Electrosprayed Salt Clusters: An Experimental/Computational Perspective. *J. Am. Soc. Mass Spectrom.* **2021**, *32* (2), 486−496.
(48) Ogorzalek Loo, R. R.; Lakshmanan, R.; Loo, J. A. What Protein Charging (and Supercharging) Reveal about the Mechanism of Electrospray Ionization. *J. Am. Soc. Mass Spectrom.* **2014**, *25* (10), 1675−1693.
(49) Abaye, D. A.; Agbo, I. A.; Nielsen, B. V. Current Perspectives on Supercharging Reagents in Electrospray Ionization Mass Spectrometry. *RSC Adv.* **2021**, *11* (33), 20355−20369.
(50) Iavarone, A. T.; Williams, E. R. Collisionally Activated Dissociation of Supercharged Proteins Formed by Electrospray Ionization. *Anal. Chem.* **2003**, *75* (17), 4525−4533.
(51) Zhang, J.; Loo, R. R. O.; Loo, J. A. Increasing Fragmentation of Disulfide-Bonded Proteins for Top-Down Mass Spectrometry by Supercharging. *Int. J. Mass Spectrom.* **2015**, *377*, 546−556.
(52) Julian, R. R. The Mechanism Behind Top-Down UVPD Experiments: Making Sense of Apparent Contradictions. *J. Am. Soc. Mass Spectrom.* **2017**, *28* (9), 1823−1826.
(53) Crittenden, C. M.; Novelli, E. T.; Mehaffey, M. R.; Xu, G. N.; Giles, D. H.; Fies, W. A.; Dalby, K. N.; Webb, L. J.; Brodbelt, J. S. Structural Evaluation of Protein/Metal Complexes via Native Electrospray Ultraviolet Photodissociation Mass Spectrometry. *J. Am. Soc. Mass Spectrom.* **2020**, *31* (5), 1140−1150.
(54) Cammarata, M. B.; Thyer, R.; Rosenberg, J.; Ellington, A.; Brodbelt, J. S. Structural Characterization of Dihydrofolate Reductase Complexes by Top-Down Ultraviolet Photodissociation Mass Spectrometry. *J. Am. Chem. Soc.* **2015**, *137* (28), 9128−9135.
(55) Klein, D. R.; Holden, D. D.; Brodbelt, J. S. Shotgun Analysis of Rough-Type Lipopolysaccharides Using Ultraviolet Photodissociation Mass Spectrometry. *Anal. Chem.* **2016**, *88* (1), 1044−1051.
(56) Juetten, K. J.; Brodbelt, J. S. MS-TAFI: A Tool for the Analysis of Fragment Ions Generated from Intact Proteins. *J. Proteome Res.* **2023**, *22*, 546.
(57) Liu, J.; McLuckey, S. A. Electron Transfer Dissociation: Effects of Cation Charge State on Product Partitioning in Ion/Ion Electron Transfer to Multiply Protonated Polypeptides. *Int. J. Mass Spectrom.* **2012**, *330−332*, 174−181.
(58) Hauser, N. J.; Basile, F.; Han, H.; McLuckey, S. A. Electron Transfer Dissociation of Peptides Generated by Microwave D-Cleavage Digestion of Proteins. *J. Proteome Res.* **2008**, *7* (5), 1867−1872.
(59) James, V. K.; Sanders, J. D.; Aizikov, K.; Fort, K. L.; Grinfeld, D.; Makarov, A.; Brodbelt, J. S. Advancing Orbitrap Measurements of Collision Cross Sections to Multiple Species for Broad Applications. *Anal. Chem.* **2022**, *94* (45), 15613−15620.

https://doi.org/10.1021/jasms.3c00138
J. Am. Soc. Mass Spectrom. 2023, 34, 1467−1476